INTERNATIONAL JOURNAL FOR NUMERICAL METHODS IN FLUIDS
Int. J. Numer. Meth. Fluids 2007; **55**:1121–1141
Published online 3 May 2007 in Wiley InterScience (www.interscience.wiley.com). DOI: 10.1002/fld.1505

On the selective local stabilization of the mixed Q1–P0 element

Jinshui Qin[1] and Shangyou Zhang[2,*,†]

[1]*10321 Yellow Pine Dr., Vienna, VA 22182, U.S.A.*
[2]*Department of Mathematical Sciences, University of Delaware, Newark, DE 19716, U.S.A.*

SUMMARY

In this paper we study the stability and performance of the quadrilateral finite element $\mathcal{Q}_1$–$\mathcal{P}_0$ (bilinear/constant) for the Stokes equations. We set up a framework to show the stability of the element for a wide range of meshes with macroelement patches. We apply the new theory to show the stability of $\mathcal{Q}_1$–$\mathcal{P}_0$ elements on some previously studied meshes and on some newly suggested meshes. Nevertheless such earlier and newly suggested meshes are not effective in practice, compared to the traditional unstable meshes for the $\mathcal{Q}_1$–$\mathcal{P}_0$ element. The new theory leads naturally to a general idea in treating instability of square $\mathcal{Q}_1$–$\mathcal{P}_0$ elements by the local stabilization on macroelement patches of larger, but fixed sizes. The good performance of the traditional $\mathcal{Q}_1$–$\mathcal{P}_0$ square elements with filtering can be kept in some cases after the local stabilization. Some numerical tests are provided to support the theory and to show the performance of stabilized $\mathcal{Q}_1$–$\mathcal{P}_0$ elements. Copyright © 2007 John Wiley & Sons, Ltd.

Received 11 March 2007; Accepted 13 March 2007

KEY WORDS: quadrilateral finite elements; mixed finite elements; Stokes equations

1. INTRODUCTION

The $\mathcal{Q}_1$–$\mathcal{P}_0$ element is a type of quadrilateral element for the Stokes equations, where we use continuous piecewise 'bilinear' approximation for the velocity and discontinuous piecewise constant approximation for the pressure. The simplicity and the 'well-balanced' velocity and pressure spaces of this element make it one of the most popularly used elements in computations for incompressible flows. This element is unstable in general, however, it does perform well in practical computations in terms of the good velocity approximation and a good recovered pressure. There is a vast amount of literature on the stability and performance of this element. One quotation from Brezzi and Fortin's book [1, Section VI.3] well addresses this element: 'However simple it may

*Correspondence to: Shangyou Zhang, Department of Mathematical Sciences, University of Delaware, Newark, DE 19716, U.S.A.
†E-mail: szhang@udel.edu

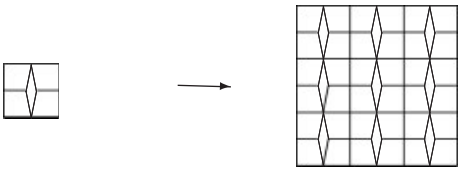

Figure 1. Earlier proposed method—B_h macroelement patch everywhere.

look, the $\mathcal{Q}_1$–$\mathcal{P}_0$ element is one of the hardest elements to analyze and many questions are still open about its properties'. For more history of this element please see [1, 2].

The stability of this element is strongly mesh dependent. Namely, the inf–sup condition (or BB condition) established in [3, 4] holds on some meshes but fails on others. The most amazing part of this element is that it always gives good velocity approximation although the inf–sup condition may not be satisfied. A good pressure can be recovered by filtering out some 'local spurious' pressure modes from the pressure approximation, if necessary. For some meshes the pressure is so good that no postprocessing is needed. Like all other unstable elements, the more irregular the mesh is, the better stability the $\mathcal{Q}_1$–$\mathcal{P}_0$ element gives. Thanks to the work of [5–14] we understand more about the mechanism of the stability and approximability of the $\mathcal{Q}_1$–$\mathcal{P}_0$ element. For summary of the known results on this element please read [1, 2].

Most of the known theoretical results of this element are limited to the rectangular meshes of some very regular domain. It is known, on the square mesh of the unit square with mesh size h, that the reduced inf–sup constant is Ch. Therefore, the stability and convergence theorem by Brezzi [4] cannot been applied directly. However, the element does provide the optimal velocity approximation and an optimal pressure solution too with possibly filtering out some spurious pressure modes. As regards the irregular quadrilateral meshes, there are a very few available theoretical results. Stenberg *et al.* [11, 15] studied two mesh families for the $\mathcal{Q}_1$–$\mathcal{P}_0$ element: one is stable and one unstable (see Figure 1 for the stable mesh). It has been proven that both families provide an optimal velocity approximation.

In this paper, we devote our effort to the following two issues: first to set a general framework in which a wide range of stable mesh families of $\mathcal{Q}_1$–$\mathcal{P}_0$ can be constructed, and secondly, to investigate the stability mechanism of the element by perturbing square meshes of the unit square. For the $\mathcal{Q}_1$–$\mathcal{P}_0$ element, the dimension of the space of the nontrivial spurious pressure modes (global constant functions are the trivial ones) usually is at most 1, and most of the time is 0 for irregular meshes. For instance, on a square mesh of the unit square, the nontrivial spurious pressure modes are multiples of the 'checkerboard' mode. If the dimension is zero, then the inf–sup constant is positive—however, this is not enough to guarantee a successful stability analysis. For example, perturbing only one node of a square mesh would make the discrete pressure space having no spurious pressure modes while the inf–sup constant is Ch or smaller. Therefore, not only the spurious pressure modes block our analysis, but also, even more severe, the bad pressure modes make the inf–sup or reduced inf–sup constant very small. All these bad modes are due to certain mesh structures. A natural thought is to control the mesh structure such that all these bad modes have no chance to appear in the pressure space. To this end, we construct some special submeshes that have the power to eliminate the bad modes if these submeshes are distributed evenly in arbitrary quadrilateral meshes. Applying this idea gives many stable mesh families for the $\mathcal{Q}_1$–$\mathcal{P}_0$ element. An alternative way of eliminating the bad modes in the pressure is to perturb

DOI: 10.1002/fld

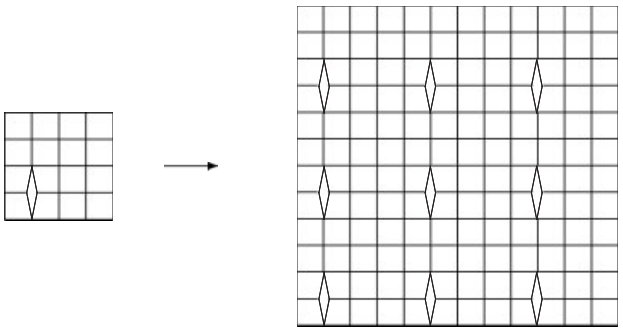

Figure 2. Putting one B_h macroelement in each patch of four $\mathscr{M}_{2h}$ squares.

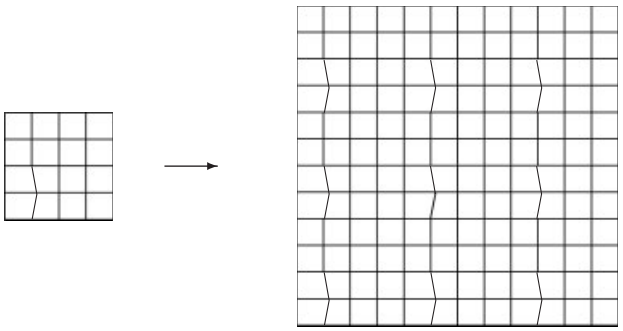

Figure 3. Perturbing one centre point out of each patch of 16 squares.

regular meshes or to modify the finite element space slightly. We do not only want to eliminate the bad modes but also to increase the lower bound of the inf–sup condition.

To be more specific on the above-mentioned two ideas on stabilization, let us see some meshes for the $\mathscr{Q}_1$–$\mathscr{P}_0$ element. Instead of using macroelements everywhere as shown in Figure 1, we can use only one such pattern on a big patch as shown in Figure 2. Figure 2 mesh requires less computation compared with that on the mesh in Figure 1, but produces better results (see Section 6), while in both cases the inf–sup condition holds. For the second idea, we perturb only one vertex on each local patch of regular meshes, shown in Figure 3. Compared to the meshes in Figure 2, the type of mesh of Figure 3 requires even less computation but would produce better results in general. Extending this idea of local stabilization further, to achieve the good performance (with filtering) of the unstable $\mathscr{Q}_1$–$\mathscr{P}_0$ element on uniform meshes, we then either add a bubble function on each macroelement patch to the discrete velocity space, shown in Figure 4, or eliminate a free variable of the discrete pressure space on each patch, shown in Figure 5. By using either method, we obtain the inf–sup condition (with a positive lower bound) while keeping the good numerical performance of the unstable element.

We need to emphasize that the term 'stabilizing the $\mathscr{Q}_1$–$\mathscr{P}_0$ element' is completely different from its usage elsewhere. It is true that the term 'stabilization' is meant to modify the weak form of the divergence-free equation by adding a lower order bilinear form on the pressure space or

DOI: 10.1002/fld

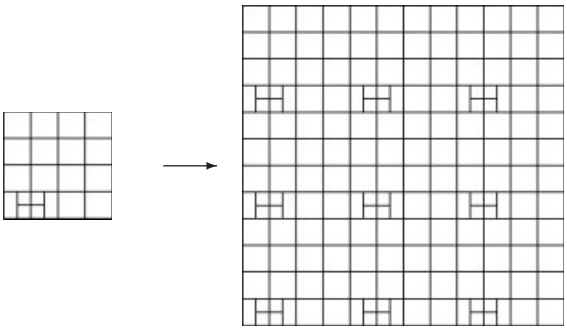

Figure 4. Adding one bubble to the velocity on each patch of 16 squares.

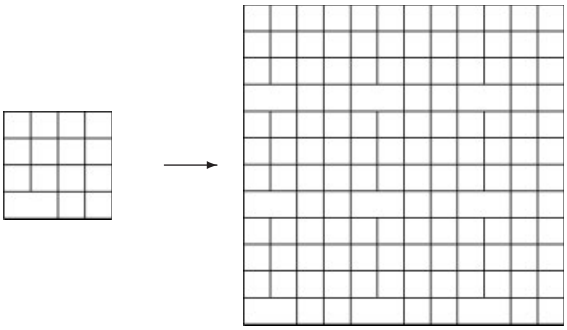

Figure 5. Combining two discrete pressure freedoms (uniform grids for the velocity).

some discrete forms, for example, cf. [1, 2]. In particular, such stabilizations on the $\mathscr{Q}_1$–$\mathscr{P}_0$ element were studied in detail by Eguchi [16], Silvester and Kechkar [17], and Hughes and Franca [18]. But in this paper, we modify meshes to get stable $\mathscr{Q}_1$–$\mathscr{P}_0$ elements when we do 'stabilization'.

In this paper, the stability analysis of the mixed element is based on the so-called macroelement technique originated from the work of [5, 15, 19]. There are many versions of the macroelement technique (cf. [1, 2, 5, 15, 19–21]). We use the two versions developed in [21] in our analysis.

The rest of the paper is organized as follows. In Section 2 we briefly introduce the mixed formulation of Stokes equations and the definition of the $\mathscr{Q}_1$–$\mathscr{P}_0$ element. In Section 3 we introduce two theorems of the macroelement techniques for checking the stability of mixed finite element methods. In Section 4 we set up a general framework for constructing stable mesh families for the $\mathscr{Q}_1$–$\mathscr{P}_0$ element; many stable mesh families are presented and analysed based on the framework in this section. In Section 5 we study the effect of mesh perturbation on the stability of the $\mathscr{Q}_1$–$\mathscr{P}_0$ element. Finally, in Section 6 we report some numerical results.

2. THE $\mathscr{Q}_1$–$\mathscr{P}_0$ ELEMENT FOR STOKES EQUATIONS

In this section we briefly introduce the mixed formulation of Stokes equations, stability or reduced stability of a mixed finite element, and the definition of the element $\mathscr{Q}_1$–$\mathscr{P}_0$.

DOI: 10.1002/fld

For the stationary Stokes equations, we solve for $(\mathbf{u}, p) \in (\mathbf{V} \times P) := \mathbf{H}_0^1(\Omega) \times L^2(\Omega)$ in the following system:

$$\begin{aligned} -\Delta \mathbf{u} + \nabla p &= \mathbf{f} \quad \text{in } \Omega \\ \operatorname{div} \mathbf{u} &= 0 \quad \text{in } \Omega \\ \mathbf{u} &= 0 \quad \text{on } \partial\Omega \end{aligned} \tag{1}$$

Here $\mathbf{u} = (u_1, u_2)$ is the velocity of the fluid, p is the pressure, $\mathbf{f} = (f_1, f_2)$ is the external force, and Ω is a polygonal domain in $\mathbf{R}^2$. If we let $\mathbf{V}_h \times P_h \subset \mathbf{V} \times P$ denote a finite element space, then an approximated solution $(\mathbf{u}_h, p_h) \in \mathbf{V}_h \times P_h$ of $(\mathbf{u}, p)$ is sought from the following discrete weak formulation of (1):

$$\begin{aligned} \int_\Omega \nabla \mathbf{u}_h : \nabla \mathbf{v} - \int_\Omega p_h \operatorname{div} \mathbf{v} &= \int_\Omega \mathbf{f} \cdot \mathbf{v} \quad \forall \mathbf{v} \in \mathbf{V}_h \\ \int_\Omega q \operatorname{div} \mathbf{u}_h &= 0 \quad \forall q \in P_h \end{aligned} \tag{2}$$

Here the parameter h refers to the mesh size.

The properties of the uniqueness and convergence of the finite element solution of (2) are established in the following theorem, see Babuška [3] and Brezzi [4].

Theorem 2.1
Suppose the finite element spaces $\mathbf{V}_h$ and P_h satisfy the inf–sup (or BB, or LBB) condition

$$\gamma_h(\mathbf{V}_h, P_h) := \inf_{0 \neq p \in \hat{P}_h} \sup_{0 \neq \mathbf{v} \in \mathbf{V}_h} \frac{\int_\Omega p \operatorname{div} \mathbf{v}}{\|\mathbf{v}\|_{1,\Omega} \|p\|_{0,\Omega}}$$

then system (2) has a unique solution $(\mathbf{u}_h, p_h) \in (\mathbf{V}_h, \hat{P}_h)$ satisfying

$$\|\mathbf{u} - \mathbf{u}_h\|_{1,\Omega} + \|p - p_h\|_{0,\Omega} \leqslant C \inf_{\mathbf{v} \in \mathbf{V}_h, q \in P_h} (\|\mathbf{u} - \mathbf{v}\|_{1,\Omega} + \|p - q\|_{0,\Omega})$$

where $(\mathbf{u}, p)$ is the solution of (1), $\hat{P}_h = \{q \in P_h \mid \int_\Omega q = 0\}$, and C is a positive constant depending on γ_h.

The constant $\gamma_h(\mathbf{V}_h, P_h)$ is called the inf–sup constant. A finite element $\mathbf{V}_h \times P_h$ is said to be stable on a mesh family if $\gamma_h(\mathbf{V}_h, P_h)$ is bounded below by a positive number independent of h; otherwise the element is said to be unstable. For convenience, we define

$$\begin{aligned} N_h &= \left\{ p \in P_h \,\middle|\, \int_\Omega p \operatorname{div} \mathbf{v} = 0 \ \forall \mathbf{v} \in \mathbf{V}_h \right\} \\ M_h &= \text{the } L^2\text{-orthogonal complement of } N_h \text{ in } P_h \end{aligned} \tag{3}$$

DOI: 10.1002/fld

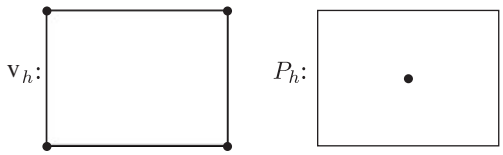

Figure 6. The nodal variables of the $\mathscr{Q}_1$–$\mathscr{P}_0$ element.

On a mesh family an element $\mathbf{V}_h \times P_h$ is said to be *reduced-stable* if $\dim N_h > 1$ and $\mathbf{V}_h \times M_h$ is stable. The constant $\gamma_h(\mathbf{V}_h, M_h)$ is called a *reduced inf–sup constant*. We note that $\mathbf{V}_h \times P_h$ and $\mathbf{V}_h \times M_h$ provide the same velocity approximation.

Let $\mathscr{Q}_h$ denote a quadrilateral partition of the domain Ω, where h is the length of the maximum edges in $\mathscr{Q}_h$. For any $T \in \mathscr{Q}_h$, we denote h_T (resp. ρ_T) the longest (resp. shortest) edge of T, $\theta_{i,T}$, $i = 1, 2, 3, 4$, the angles of T. A family of quadrilateral meshes is said to satisfy the shape condition if there exists $\sigma > 1$ and $0 < \kappa < 1$ such that

$$h_T \leqslant \sigma \rho_T, \quad |\cos \theta_{i,T}| \leqslant \kappa, \quad i = 1, 2, 3, 4 \tag{4}$$

for all T in the meshes of the family. Let $\hat{T}$ denote the unit square $[0, 1] \times [0, 1]$ with vertices $\hat{t}_1$, $\hat{t}_2$, $\hat{t}_3$, and $\hat{t}_4$ (counted counterclockwise). For any quadrilateral $T \in \mathscr{Q}_h$ with the vertices t_1, t_2, t_3, and t_4 (counterclockwise), there exists exactly one invertible bilinear mapping $F_T \in \hat{Q}_1(\hat{T})^2$ ($\hat{Q}_k(\hat{T}) = \{\sum_{0 \leqslant i,j \leqslant k} a_{ij} \hat{x}^i \hat{y}^j \mid a_{ij} \in \mathbf{R}\}$) that maps $\hat{T}$ onto T such that $F_T(\hat{t}_i) = t_i$.

The definition of the $\mathscr{Q}_1$–$\mathscr{P}_0$ element reads

$$\begin{aligned} \mathbf{V}_h &= \{\mathbf{v} \in \mathbf{H}_0^1(\Omega) \mid \mathbf{v}|_T = \hat{\mathbf{v}} \circ F_T^{-1}, \hat{\mathbf{v}} \in \hat{Q}_1(\hat{T})^2, T \in \mathscr{Q}_h\} \\ P_h &= \{q \in L^2(\Omega) \mid q|_T = \hat{q} \circ F_T^{-1}, \hat{q} \in \hat{Q}_0(\hat{T}), T \in \mathscr{Q}_h\} \end{aligned} \tag{5}$$

The degrees of freedom of this element are depicted in Figure 6.

3. THE MACROELEMENT TECHNIQUE

In this section, we briefly introduce two theorems of the macroelement technique for checking the stability of mixed finite element methods for Stokes equations. They are the so-called macroelement partition theorem and macroelement covering theorem [20, 21]. In addition, some concepts relevant to the stability analysis shall be introduced in this section, too. For more detailed discussions or proofs please see [20, 21].

Given a quadrilateral grid $\mathscr{Q}_h$ of a polygonal domain Ω, a macroelement with respect to $\mathscr{Q}_h$ is a polygonal region U formed by some quadrilaterals in $\mathscr{Q}_h$. A macroelement covering is a covering of $\mathscr{Q}_h$ by macroelements. Such a covering is called a macroelement partition if the intersection of a pair of distinct, nondisjoint macroelements is either a single vertex of $\mathscr{Q}_h$ or a connected set consisting of some edges of the quadrilateral mesh. In other words, the difference between partition and covering is whether a macroelement covering overlaps. We denote a macroelement partition or covering by $\mathscr{U}_h$. In this paper we assume that all the quadrilateral meshes satisfy the shape condition (4).

DOI: 10.1002/fld

For a macroelement U we define localizations to U of the finite element spaces $\mathbf{V}_h$, P_h, N_h, and M_h as follows:

$$\begin{aligned} \mathbf{V}_h^U &= \{\mathbf{v} \in \mathbf{V}_h \mid \operatorname{supp} \mathbf{v} \subset U\} \\ P_h^U &= \{\chi^U p \mid p \in P_h\} \\ N_h^U &= \left\{ p \in P_h^U \,\middle|\, \int_\Omega p \operatorname{div} \mathbf{v} = 0 \ \forall \mathbf{v} \in \mathbf{V}_h^U \right\} \\ M_h^U &= \text{the } L^2\text{-orthogonal complement of } N_h^U \text{ in } P_h^U \end{aligned} \tag{6}$$

Here χ^U denotes the characteristic function of U and $\operatorname{supp} \mathbf{v}$ is the support of $\mathbf{v}$.

The macroelement partition theorem is based on local stabilities over macroelements and the stability of a special element over the whole domain. It is a useful tool to check the inf–sup condition of a mixed finite element on meshes formed by certain patterns.

Theorem 3.1 (*Macroelement partition theorem*)
Let $\mathscr{U}_h$ be a macroelement partition of Ω with respect to some quadrilateral mesh $\mathscr{Q}_h$. Let $\mathbf{V}_h \times P_h$ be a finite element space defined on $\mathscr{Q}_h$, and let

$$Q_h := \left\{ q \in \sum_{U \in \mathscr{U}_h} N_h^U \,\middle|\, \int_\Omega q r = 0 \ \forall r \in N_h \right\}$$

If $\gamma(\mathbf{V}_h, Q_h) > 0$, then the reduced inf–sup constant $\gamma(\mathbf{V}_h, M_h)$ is strictly positive. Moreover, if α is a positive lower bound for $\gamma(\mathbf{V}_h, Q_h)$ and $\gamma(\mathbf{V}_h^U, M_h^U)$ for all $U \in \mathscr{U}_h$, then $\gamma(\mathbf{V}_h, M_h)$ can be bounded below by a positive constant depending only on α.

In order to present the theory on overlapping macroelement coverings we need to assume an approximation property of the velocity space $\mathbf{V}_h$ (cf. [2, 15, 19] that (7) holds for all quasi-uniform elements): for each $\mathbf{w} \in \mathbf{H}_0^1(\Omega)$ there exists a function $\mathbf{w}_h \in \mathbf{V}_h$ such that

$$\sum_{T \in \mathscr{Q}_h} h_T^{-2} \|\mathbf{w} - \mathbf{w}_h\|_{0,T}^2 + \sum_{e \in \mathscr{E}_h} h_e^{-1} \|\mathbf{w} - \mathbf{w}_h\|_{0,e}^2 + \|\mathbf{w}_h\|_{1,\Omega}^2 \leqslant C \|\mathbf{w}\|_{1,\Omega}^2 \tag{7}$$

where h_T is the diameter of T, h_e is the length of e, and C is a positive number independent of h. Given a macroelement covering $\mathscr{U}_h$ of Ω, for any internal edge $e \in \overset{o}{\mathscr{E}}_h$ (the set of all internal edges of $\mathscr{Q}_h$), we define L_e to be the number of macroelements in $\mathscr{U}_h$ that contain e as one interior edge. The covering is said to possess the *overlap property* if $C_c := \min\{L_e \mid e \in \overset{o}{\mathscr{E}}_h\} \geqslant 1$. The quantity C_c is called the covering constant of $\mathscr{U}_h$. The macroelement covering theorem below is more flexible and powerful than the partition theorem above in terms of the choice of macroelements. More quadrilateral meshes can be treated by this theorem.

Theorem 3.2 (*Macroelement covering theorem*)
Let $\mathscr{U}_h$ be a macroelement covering of a quadrilateral mesh $\mathscr{Q}_h$ satisfying the overlap property. If $\mathbf{V}_h$ satisfies (7) and

$$\chi^U p \in M_h^U + \mathbf{R}\chi^U \quad \forall p \in M_h$$

DOI: 10.1002/fld

then the reduced inf–sup constant $\gamma(\mathbf{V}_h, M_h)$ is strictly positive. Here and later $\mathbf{R}$ stands for the set of constants. Moreover, if for each $U \in \mathscr{U}_h$ the inf–sup constant $\gamma(\mathbf{V}_h^U, M_h^U) \geqslant \alpha > 0$, then $\gamma(\mathbf{V}_h, M_h)$ can be bounded below by a positive constant depending only on α and the covering constant for $\mathscr{U}_h$.

A major issue in applications of the above two theorems is to show that $\gamma_h(\mathbf{V}_h^U, M_h^U)$ is bounded below by a positive constant independent of h for all $U \in \mathscr{U}_h$. This may not be easy since $\mathscr{U}_h$ may contain macroelements with different shapes and structures. To deal with this issue more effectively, we need the concepts of equivalent macroelements and equivalence classes in our analysis following [15]. Roughly speaking, two macroelements are said to be equivalent if there is continuous piecewise linear or bilinear one-to-one mapping that maps one to another. A equivalence class of macroelements is a set of macroelements in which all macroelements are equivalent to each other. For convenience, we denote $E(U)$ the equivalence macroelement class of the macroelement U. For more detailed definitions and discussions on the concept please read [15, 19–21].

4. STABILITY ON MACROELEMENT MESHES

In this section, we set up a general framework for constructing stable mesh families for the $\mathscr{Q}_1$–$\mathscr{P}_0$ element. The main idea is to refine an irregular quadrilateral mesh by some specially designated substructures such that the stability of the element can be achieved.

Let $\mathscr{Q}_h$ denote a refinement of a quadrilateral partition $\mathscr{M}_{2h}$ of Ω. The structure of $\mathscr{M}_{2h}$ could be arbitrary. However, the structure of $\mathscr{Q}_h$ depends on how we refine the mesh $\mathscr{M}_{2h}$ into smaller quadrilaterals. To demonstrate the idea, we assume that each quadrilateral $T \in \mathscr{M}_{2h}$ is refined by either the submesh S_h or the submesh B_h showed in Figure 7. Here S_h is obtained by connecting the middle points of the four edges of T, and the structure of B_h is assumed to be unknown but fixed for the time being. The four middle points of edges of T are certain to be the nodes of $\mathscr{Q}_h$. We denote T^B (resp. T^S) the refinement of the quadrilateral $T \in \mathscr{M}_{2h}$ by B_h (resp. S_h).

Lemma 4.1

Let $\mathscr{M}_{2h}$ be a quadrilateral partition of Ω. Let $\mathscr{Q}_h$ be a refinement of $\mathscr{M}_{2h}$ where each quadrilateral of $\mathscr{M}_{2h}$ is refined by either macrostructures, S_h or B_h. Using the definitions (3), (5) and (6), if the following two conditions hold:

1. $\dim N_h^{T^B} = 1$ if $T \in \mathscr{M}_{2h}$ is partitioned by B_h;
2. at least one quadrilateral $T \in \mathscr{M}_{2h}$ is partitioned by B_h,

then

$$\dim N_h = 1$$

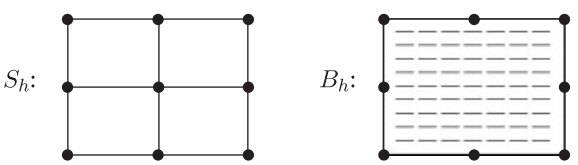

Figure 7. Two types of refinements used on $\mathscr{M}_{2h}$ to obtain $\mathscr{Q}_h$.

DOI: 10.1002/fld

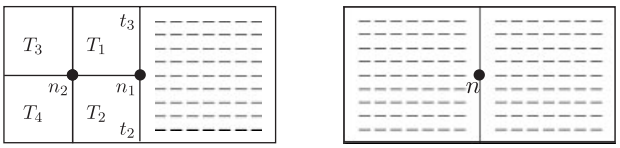

Figure 8. Two types of macroelements of $\mathscr{M}_{2h}$.

Proof

Let the union of any two quadrilaterals, which share one common edge, of $\mathscr{M}_{2h}$ be a macroelement of $\mathscr{M}_{2h}$. The collection of all such macroelements forms a macroelement covering of $\mathscr{M}_{2h}$, denoted by $\mathscr{O}_{2h}$. By refining all the macroelements of $\mathscr{O}_{2h}$, we obtain a macroelement covering of $\mathscr{Q}_h$, denoted by $\mathscr{U}_h$. Let $U = W_1 \cup W_2 \in \mathscr{O}_{2h}$ be arbitrary, where W_1 and W_2 are two quadrilaterals of $\mathscr{M}_{2h}$. Since each of W_1 and W_2 can be refined by either B_h or S_h, there are four combinations. For convenience, we let $U_1 = W_1^S \cup W_2^B$, $U_2 = W_1^B \cup W_2^B$, $U_3 = W_1^B \cup W_2^S$, $U_4 = W_1^S \cup W_2^S$. The macroelements U_1 and U_2 are depicted in Figure 8.

First we shall show

$$\dim N_h^{U_i} = 1, \quad i = 1, 2, 3$$

Namely, we need to show that if $q \in N_h^{U_i}$ satisfies

$$\int_{U_i} q \operatorname{div} \mathbf{v} = 0 \quad \forall \mathbf{v} \in \mathbf{V}_h^{U_i} \tag{8}$$

then q is a piece of constant on the whole U_i, i.e. any $q \in N_h^{U_i}$ must be constant on these three types of macroelements.

We consider the first case. Let $q \in N_h^{U_1}$ be arbitrary. For convenience, we assume, cf. Figure 8, $q|_{T_1} = c_1$, $q|_{T_2} = c_2$, and $q|_{W_2^B} = c$ (because of $\dim N_h^{B_h} = 1$). Let ϕ_1 denote the nodal basis function corresponding to the node n_1 of U_1 (see Figure 8). The linear system (8) implies

$$\int_{T_1 \cup T_2 \cup W_2} q \operatorname{div} \begin{pmatrix} r_1 \phi_1 \\ r_2 \phi_1 \end{pmatrix} = 0 \quad \forall r_1, r_2 \in \mathbf{R} \tag{9}$$

We do not know the refinement of the big square W_2^B yet, and neither the shape function ϕ_1 inside W_2^B. To compute integral (9) on W_2, we have to use then the Green's formula to convert the area integral to an integral on the boundary. By doing so, noting that q is piecewise constant, we conclude that (9) is equivalent to the following two equations:

$$\begin{aligned} (c_2 - c_1) \int_{n_2 n_1} \phi_1 \, \mathrm{d}x = 0 \\ (c_1 - c) \int_{n_1 t_3} \phi_1 \mathrm{d}y + (c_2 - c) \int_{t_2 n_1} \phi_1 \mathrm{d}y = 0 \end{aligned} \tag{10}$$

DOI: 10.1002/fld

Since ϕ_1 is linear on each of the three edges in the integral of (10) and it runs from 1 to 0 on each edge, we get immediately from the first equation that $c_1 = c_2$ and then from the second equation of (10) that $c = c_1 = c_2$. This leads to the trivial solution, i.e. q is one constant on the big rectangle $T_1 \cup T_2 \cup W_2^B$. Repeating the above arguments to the next two small squares T_3 and T_4 plus the big rectangle $T_1 \cup T_2 \cup W_2^B$, where we would replace the nodal basis function ϕ_1 by ϕ_2 at node n_2 (see Figure 8), we conclude that q is a constant on the whole U_1 if $q \in N_h^{U_1}$. Namely

$$\dim(N_h^{U_1}) = \dim(N_h^{W_1^S \cup W_2^B}) = \dim(N_h^{T_1 \cup T_2 \cup T_3 \cup T_4 \cup W_2^B}) = 1$$

Next, we shall prove $\dim N_h^{U_2} = 1$. Let $q \in N_h^{U_2}$ be arbitrary. We may assume that $q|_{W_1^B} = c_1$ and $q|_{W_2^B} = c_2$, since $\dim N_h^{W_i^B} = 1$, for $i = 1, 2$, see Figure 8. Let ϕ_1 denote the nodal basis function corresponding to the internal node n of U_2 in Figure 8. From (8) we have

$$c_1 \int_{W_1^B} \operatorname{div} \begin{pmatrix} r_1\phi_1 \\ r_2\phi_1 \end{pmatrix} + c_2 \int_{W_2^B} \operatorname{div} \begin{pmatrix} r_1\phi_1 \\ r_2\phi_1 \end{pmatrix} = 0 \quad \forall r_1, r_2 \in \mathbf{R}$$

Again, we do not know the construction of W_1^B and W_2^B yet. So we convert the area integrals above to boundary integrals as before. If follows that

$$(c_1 - c_2) r_1 \int_{\overline{W_1^B} \cap \overline{W_2^B}} \phi_1 \, \mathrm{d}y = 0$$

Therefore, $c_2 = c_1$ and $\dim N_h^{U_2} = 1$.

The proof of $\dim N_h^{U_3} = 1$ is the same as that of $\dim N_h^{U_1} = 1$.

Finally, we deal with the macroelement U_4. It is true that $N_h^{U_4}$ does contain a checkerboard mode and that $\dim N_h^{U_4} > 1$. However, we assumed there is at least one $T \in \mathscr{M}_{2h}$ refined by B_h, i.e. at least there is one W^B which is refined into a T^B in $\mathscr{Q}_h$. Therefore if $q \in N_h$, then q is a constant on such a region T^B by the assumption 1 in the lemma. By the analysis above for U_1 and U_2, we know that q assumes the same constant value on the (four, or less at the boundary) neighbouring $\mathscr{M}_{2h}$ squares of the W^B (T^B is a refinement of this W^B). Such a propagation would not stop until we reach the conclusion that q is a constant on the whole domain Ω. That is

$$\dim N_h = 1 \qquad \square$$

For simplicity, we introduce the following notations. For any vertex $s \in \mathscr{M}_{2h}$, we define G_s the polygonal region formed by the union of all $\mathscr{M}_{2h}$ quadrilaterals on which s is a vertex. For any given vertex $v \in \mathscr{M}_{2h}$, we recursively define $R_v(k)$, the kth set of vertices, and $D_v(k)$, the level k macroelement of $\mathscr{M}_{2h}$, as follows:

$$R_v(0) = \{v\}$$

$$D_v(0) = G_v$$

DOI: 10.1002/fld

$$R_v(k) = \{\text{all vertices of } D_v(k-1)\}, \quad k = 1, 2, \ldots$$

$$D_v(k) = \bigcup_{s \in R_v(k)} G_s, \quad k = 1, 2, \ldots$$

Theorem 4.1
Let a family of quadrilateral meshes $\mathscr{M}_{2h}$, $h>0$ on Ω satisfy the shape condition (4). Let $\mathscr{Q}_h$ be a mesh of quadrilaterals refined from $\mathscr{M}_{2h}$ by either B_h or S_h. If the following two conditions hold:

(a1) there is a fixed integer $k>0$ such that for each vertex v of $\mathscr{M}_{2h}$ at least one quadrilateral contained in $D_v(k)$ is partitioned by B_h;
(a2) denoting by $E(B_h)$ the macroelement equivalence class of B_h

$$\dim N_h^U = 1 \quad \forall U \in E(B_h)$$

then the $\mathscr{Q}_1$–$\mathscr{P}_0$ is stable on the family of meshes $\mathscr{Q}_h$, $h>0$, and the inf–sup constant γ_h is bounded below by a positive number depending only on the structure of B_h, k, σ, and κ.

Proof
To prove this theorem we shall apply the macroelement covering theorem (Theorem 3.2). To this end, we need to check the following five conditions:

(C1) $\dim N_h = 1$;
(C2) approximation property (7) holds;
(C3) there exists a macroelement covering $\mathscr{U}_h$ of $\mathscr{Q}_h$ satisfying the overlap property;
(C4) $\dim N_h^U = 1$ for all macroelement $U \in \mathscr{U}_h$;
(C5) there exists $\alpha>0$ independent of h such that

$$\gamma_h(\mathbf{V}_h^U, M_h^U) \geqslant \alpha \quad \forall U \in \mathscr{U}_h$$

Clearly, (C1) holds because of Lemma 4.1 and the assumption (a1) of the theorem.

As regards (C2), it holds for the finite element space $\mathbf{V}_h$ defined in (4), see [2, 19, 22, 23].

By the definition, $D_v(k)$ is a macroelement of $\mathscr{M}_{2h}$. If we set

$$\mathscr{O}_{2h} = \{D_v(k) \mid \text{for all vertices } v \text{ of } \mathscr{M}_{2h}\}$$

then it is a macroelement covering of $\mathscr{M}_{2h}$ satisfying the overlap property. Any macroelement $U \in \mathscr{O}_{2h}$ is also formed by some quadrilaterals of $\mathscr{Q}_h$, therefore U is a macroelement of $\mathscr{Q}_h$. Thus, associated with $\mathscr{O}_h$ we have a macroelement covering $\mathscr{U}_h$ of $\mathscr{Q}_h$ satisfying the overlap property. According to the definitions of $\mathscr{O}_{2h}$ and $\mathscr{U}_h$, by the assumption (a1), any macroelement $U \in \mathscr{U}_h$ (refinement of some macroelement of $\mathscr{O}_{2h}$) contains at least one submesh B_h. Therefore, applying Lemma 4.1, we get

$$\dim N_h^U = 1$$

By the shape condition (4), the definitions of $\mathscr{O}_{2h}$ and $\mathscr{U}_h$, the definitions of S_h and B_h, the number of different equivalence macroelement classes of $\mathscr{U}_h$ is bounded and dependent on k, σ,

DOI: 10.1002/fld

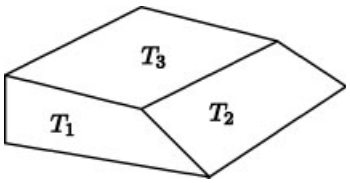

Figure 9. A macroelement formed by three quadrilaterals.

and κ. According to Lemma 3.1 in [15], we conclude that (C5) holds with α dependent on k, σ, κ, and the structure of B_h.

By applying the macroelement covering theorem, we complete the proof. □

Remark 4.1

The condition (a1) of Theorem 4.1 means that the mesh structure B_h is 'uniformly' distributed in the mesh $\mathscr{Q}_h$. If the mesh $\mathscr{Q}_h$ is quasi-uniform, condition (a1) is equivalent to that for each vertex of $\mathscr{Q}_h$, there is at least one T^B, $T \in \mathscr{M}_{2h}$, contained inside the circle centred at the vertex with a radius kh, for some integer $k>0$.

Remark 4.2

The structure of B_h may be allowed to vary. Let $B_h^{(1)}, \ldots, B_h^{(m)}$ be substructures such that $\dim N_h^U = 1$ if $U = T^{B^{(i)}}$, $T \in \mathscr{M}_{2h}$, $1 \leqslant i \leqslant m$. Lemma 4.1 still holds if each quadrilateral of $\mathscr{M}_{2h}$ is partitioned by one of S_h, $B_h^{(1)}, \ldots, B_h^{(m)}$. Similarly, Theorem 4.1 holds if B_h is replaced by $B_h^{(1)}, \ldots, B_h^{(m)}$, which satisfy condition (a2), provided m is fixed.

We next consider a special type of macroelement. It is a combination of three quadrilaterals meeting at an interior vertex. The proof of next lemma can be done by a simple calculation or by referencing, for example, [15, 24].

Lemma 4.2

If a macroelement $W = T_1 \cup T_2 \cup T_3$, see Figure 9, then

$$\dim N_h^U = 1 \quad \forall U \in E(W)$$

In the rest of this section, we present some types of B_h satisfying the conditions in Theorem 4.1. The first two examples are known and analysed in [15, 24]. The analysis of all five B_h is covered by Lemma 4.2. We note that in the construction of B_h, each one must use precisely the vertices and the four mid-edge points as its boundary nodes. We remark that the resulting meshes with the help of some B_h patches would give stable $\mathscr{Q}_1$–$\mathscr{P}_0$ mixed element spaces, but the approximation of the resulting spaces, while we have more unknowns here, may be worse than that of the spaces on the uniform square meshes, though the latter does not have the inf–sup condition. This is to be illustrated by numerical examples.

Example 1 (*Stenberg* [*15*])

B_h is formed by five quadrilaterals, see the first picture of Figure 10. By Lemma 4.2, it is trivial to see $\dim N_h^U = 1$ for all $U \in E(B_h)$. Stenberg [15] proved the $\mathscr{Q}_1$–$\mathscr{P}_0$ element is stable if each quadrilateral of $\mathscr{M}_{2h}$ is partitioned by B_h—that is the special case when $k = 0$ in Theorem 4.1.

DOI: 10.1002/fld

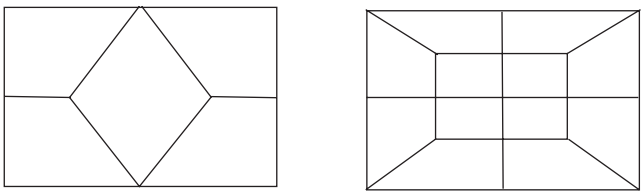

Figure 10. Two known types of B_h patches.

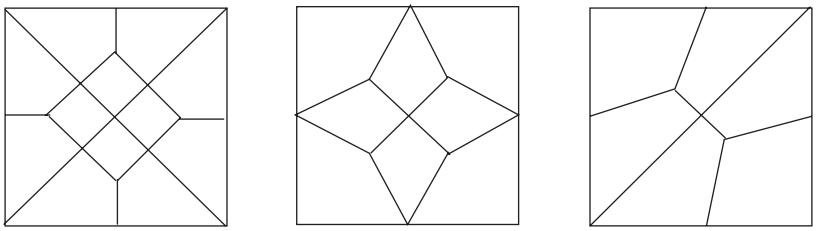

Figure 11. Three new types of B_h patches.

Example 2 (*Le Tallec and Ruas* [*24*])
B_h has the mesh structure shown in the second picture of Figure 10. Combination of Lemma 4.2 and the proof of Theorem 4.1 gives $\dim N_h^U = 1$ for all $U \in E(B_h)$.

Examples 3–5
We list three more choices of B_h in Figure 11. Each of these satisfies the second condition of Theorem 4.1. Again, from the points of implementation and the approximation property, we would list five types of B_h from the best to worst as Examples 1–5.

5. PERTURBATION OF THE SQUARE MESHES

In this section, we study the influence of perturbations of square meshes on the stability of the $\mathcal{Q}_1$–$\mathcal{P}_0$ element. To simplify the exposition, we only discuss the perturbation of square meshes of the unit square. For such square meshes, it is well known that $\dim N_h = 2$, the nontrivial spurious pressure modes are multiples of the checkerboard mode, and the reduced inf–sup constant is Ch. In this section, we will show that $\dim N_h = 1$ if one interior vertex of the square mesh is perturbed away from its original position. Furthermore, we show a stable family obtained by perturbing the square meshes of the unit square. We also generalize the idea by introducing two unusual $\mathcal{Q}_1$–$\mathcal{P}_0$ elements, one with an additional bubble velocity function on each macroelement patch, and another one with a reduction of a pressure function on each macroelement patch.

Lemma 5.1
Let $\mathcal{Q}_h$ denote a square mesh of the unit square with mesh size $h \leqslant \frac{1}{4}$. If an interior vertex of $\mathcal{Q}_h$ is perturbed away from its original position, then the $\mathcal{Q}_1$–$\mathcal{P}_0$ element has no nontrivial spurious

DOI: 10.1002/fld

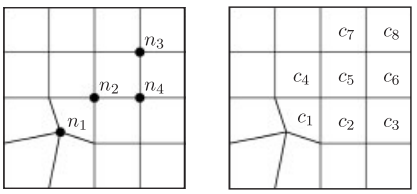

Figure 12. Perturbing one vertex on a macroelement U and the N_h^U.

pressure mode in N_h. Namely

$$\dim N_h = 1$$

Proof

We consider only the case that the lower-left corner interior vertex being moved, as shown in Figure 12. The proof for the cases that anyone of the other vertices being moved is similar.

Let p be in N_h^U, for the U being the 16 squares shown in Figure 12. Then we have

$$\int_U p \operatorname{div} \mathbf{v} = 0 \quad \forall \mathbf{v} \in \mathbf{V}_h^U \tag{11}$$

In particular, we can use, in (11), the test functions

$$\mathbf{v} = \begin{pmatrix} \phi_2 \\ 0 \end{pmatrix} \quad \text{and} \quad \mathbf{v} = \begin{pmatrix} 0 \\ \phi_2 \end{pmatrix}$$

where ϕ_2 is, as before, the $\mathcal{Q}_1$ nodal basis function at node n_2 in Figure 12. By (11), we get, after subtracting a global constant, that

$$\begin{aligned} c_2 &= -sc_1 \\ c_3 &= -tc_1 \\ c_4 &= (s + t - 1)c_1 \end{aligned}$$

Here c_i denotes the constant value of the pressure function q on some small square, as depicted in Figure 12. We note that the positive constants s and t above may be equal if the vertex n_1 is moved along the diagonal line $\overline{n_2 n_3}$. But when the vertex n_1 is perturbed

$$t \neq 1 \quad \text{and} \quad s \neq 1 \tag{12}$$

Next, we choose the test function $\mathbf{v} = (\phi_3, 0)$ and $\mathbf{v} = (0, \phi_3)$ in (11). This would lead to the following equations:

$$\begin{aligned} c_6 &= -c_5 = -(s + t - 1)c_1 \\ c_7 &= -c_5 = -(s + t - 1)c_1 \\ c_8 &= -c_7 = (s + t - 1)c_1 \end{aligned}$$

DOI: 10.1002/fld

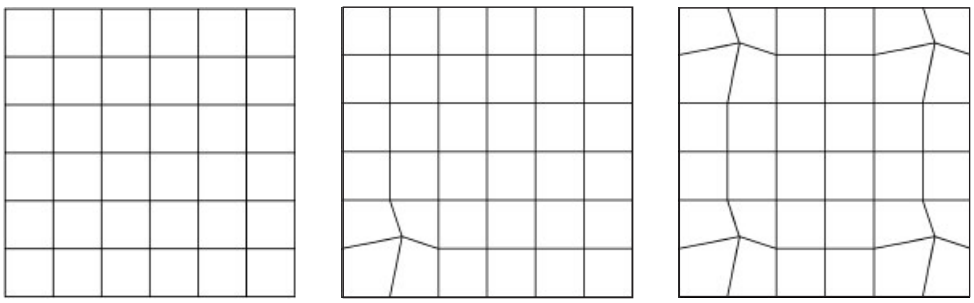

Figure 13. Square mesh, one vertex perturbation, perturbed macroelements.

Finally, let $\mathbf{v}=(\phi_4, 0)$ and $\mathbf{v}=(0, \phi_4)$ in (11), see Figure 12. A simple calculation would tell us that

$$\begin{aligned} c_6 &= -c_5 = -(s+t-1)c_1 \quad \text{(again)} \\ c_3 &= -c_6 = (s+t-1)c_1 \\ c_3 &= -c_2 = sc_1 \end{aligned}$$

The last two equations show the following two possibilities:

$$\text{either } t=1 \quad \text{or } c_1=0$$

From (12), we conclude that $c_1=0$. Therefore, as all $c_i=0$ and $p\equiv 0$ (after subtracting a global constant). So $\dim N_h^U = 1$.

Let $\mathscr{U}_h$ be the set of all the 4×4 squares of $\mathscr{Q}_h$. Clearly, $\mathscr{U}_h$ is a macroelement covering of $\mathscr{Q}_h$, and each macroelement of $\mathscr{U}_h$ is overlapped with some other macroelements. Since $\dim N_h^U = 1$ while one interior vertex of U is perturbed, the overlap property of the macroelements of $\mathscr{U}_h$ leads to $\dim N_h = 1$. Therefore, N_h consists of global constant functions only. □

Although the inf–sup constant is no longer zero if we perturb *only one* interior vertex of the square mesh $\mathscr{Q}_h$ (see Mesh B in Figure 13), it is by no means bounded below by a positive number independent of h. As a matter of fact, the inf–sup constant goes to zero as the mesh size h goes to zero. This is caused by the bad pressure modes in the pressure space. However, by the general theory established in the last section, we can bound the inf–sup constant from below, independent of h, if we perturb one interior vertex of each macroelement of a fixed size. The idea is to partition the unit square into equal squares, then partition each square into 16 quadrilaterals exactly the same way shown by the first picture in Figure 12. The resulting partition of the unit square is denoted by $\mathscr{Q}_h$, see the second picture in Figure 3. By Lemma 5.1, Theorems 3.1 and 4.1, the $\mathscr{Q}_1$–$\mathscr{P}_0$ element is stable on such a mesh family. The comments here are to be confirmed in the section of numerical test.

DOI: 10.1002/fld

6. NUMERICAL TESTS

In this section, we will first continue our investigation on the stability of the $\mathscr{Q}_1$–$\mathscr{P}_0$ element on perturbed meshes of the unit square. We investigate the (reduced) inf–sup condition number of three types of quadrilateral meshes, shown in Figure 13. Secondly, we compare the numerical results for various stabilization methods, proposed by others before and newly here.

As we proved in the previous section, perturbation of any one interior vertex of the square mesh can eliminate the checkerboard mode. In the following tests, we first move (only one) the vertex (h, h) to the point $(1.2h, 1.2h)$ (see Mesh B in Figure 13). From the computational results listed in Table I (Mesh A), we clearly see that the inf–sup constant $\bar{\gamma}_h = Ch$, i.e. $\beta = 1$ (where β is defined as $\bar{\gamma}_h = Ch^\beta$ or $\gamma_h(\mathbf{V}_h, M_h) = Ch^\beta$). Here γ_h and $\bar{\gamma}_h$ are the second (first one is zero) and the third (first two are zero) smallest eigenvalues of $M_h^{-1} B_h^T A_h^{-1} B_h$, respectively, where the three matrices are the mass matrix for pressure, the vector Laplacian matrix for velocity, and the $(\operatorname{div} \mathbf{u}_h, p_h)$ matrix. This is a well-known result for the uniform meshes that even after filtering out the checkerboard mode pressure, the inf–sup constant still goes to zero. In Table I (Mesh B), after we perturb only one vertex, the checkerboard mode pressure is no longer in N_h. Nevertheless, the mode is turned into a bad pressure mode which makes the inf–sup constant close to zero. This is shown in Table I that the value of γ_h of the Mesh B is much smaller than the reduced inf–sup constant $\gamma_h(\mathbf{V}_h, M_h)$ of the square mesh of the same mesh size.

Therefore, as we discussed in the last section, it is not enough to get $\dim N_h = 1$ by perturbing one vertex. We need to perturb one vertex on each patch of macroelement covering. This is illustrated in Mesh C of Figure 13. Here, we make sure that, among every 16 squares, one internal vertex is moved. Therefore, for h between $\frac{1}{5}$ and $\frac{1}{8}$, there are four perturbed internal vertices.

Table I. Inf–sup constants for three types of meshes in Figure 13.

	Mesh A		Mesh B		Mesh C
h	$\bar{\gamma}_h$	β	γ_h	β	γ_h
$\frac{1}{4}$	0.3676		0.0227		0.0227
$\frac{1}{5}$	0.3149	0.6929	0.0189	0.8174	0.0783
$\frac{1}{6}$	0.2740	0.7632	0.0158	0.9947	0.0621
$\frac{1}{7}$	0.2418	0.8125	0.0135	1.0101	0.0458
$\frac{1}{8}$	0.2159	0.8476	0.0118	1.0143	0.0307
$\frac{1}{9}$	0.1948	0.8725	0.0105	1.0122	0.0591
$\frac{1}{10}$	0.1774	0.8910	0.0094	1.0125	0.0542
$\frac{1}{11}$	0.1627	0.9052	0.0085	1.0110	0.0454
$\frac{1}{12}$	0.1502	0.9163	0.0078	1.0111	0.0415
$\frac{1}{13}$	0.1395	0.9252	0.0072	1.0101	0.0383
$\frac{1}{14}$	0.1302	0.9325	0.0067	1.0102	0.0320
$\frac{1}{15}$	0.1220	0.9386	0.0062	1.0096	0.0305

DOI: 10.1002/fld

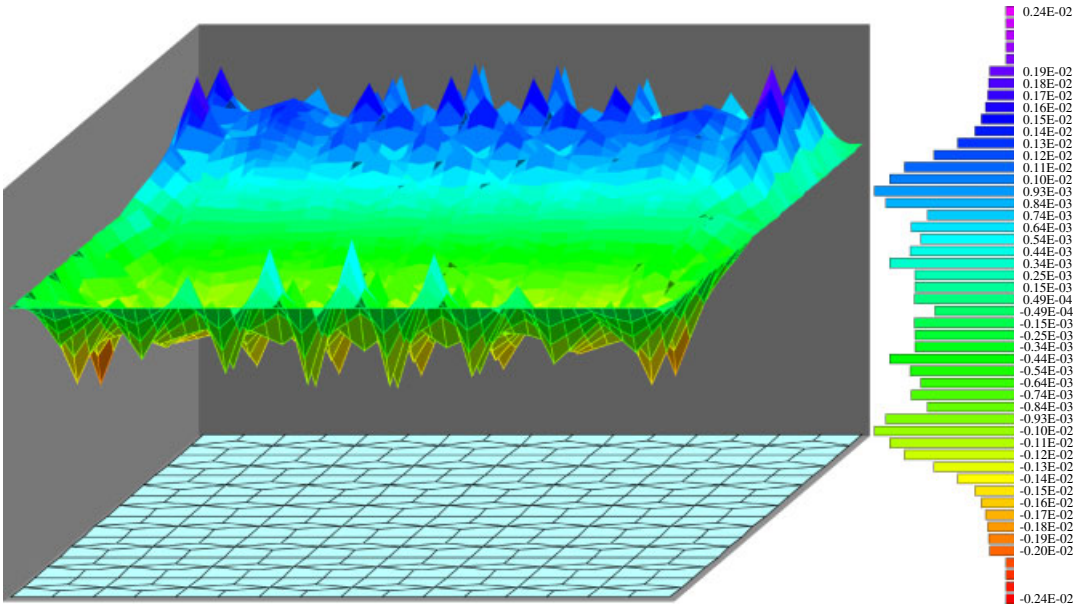

Figure 14. Error of component 1 of $\mathbf{u}_h$ on the Stenberg mesh [15].

Nine internal vertices are moved for h between $\frac{1}{9}$ and $\frac{1}{15}$. Clearly, the inf–sup constant is bounded below now, independent of h, as shown in Table I (Mesh C).

Finally, to compare various methods, numerically we solve Equation (1) where the exact solution is

$$\mathbf{u} = \mathbf{curl}\, g, \quad p = -g_{xx}, \quad g = 10(x - x^2)^2(y - y^2)^2$$

defined on the unit square $(0, 1) \times (0, 1)$. Here we know the exact solution that we can find the error between numerical solution and the exact solution easily. We first use the stable meshes as depicted in Figure 1, i.e. every $\mathscr{M}_{2h}$ squares are refined into five quadrilaterals (called a U_h macroelement). The $\mathscr{Q}_1$–$\mathscr{P}_0$ element is stable on such a mesh. This is analyzed by Stenberg [15] and we call such a mesh Stenberg mesh. The first component of error $\mathbf{u} - \mathbf{u}_h$ is plotted in Figure 14. We will compare this error with that of newly proposed method that we use only one such 5-quadrilateral B_h on a large patch of $\mathscr{M}_{2h}$ while using the standard refinement S_h on the rest $\mathscr{M}_{2h}$ squares, as shown in Figure 2. We list the several norms of errors and the orders of convergence, when using Figure 2 meshes, in the right part of Table II. Here out of eight $\mathscr{M}_{2h}$ squares one is refined into B_h while the other seven refined into S_h (see the bottom mesh in Figure 15).

We note that the newly proposed mesh, the Figure 2 mesh, provides better numerical solution with much less computation cost. To be specific, comparing the two errors in Figures 14 and 15 (by reading the bar graphs on the right of two figures), we can see that not only the peak error of the new method is much smaller but also everywhere else the new error is smaller. In this computation (please see the grids on the bottom of Figures 14 and 15), the number of nodal variables for the discrete velocity space is 578 for the Stenberg mesh, while it is only 466 for the Figure 2 mesh.

DOI: 10.1002/fld

Table II. Convergence of $\mathscr{Q}_1$–$\mathscr{P}_0$ on uniform or stabilized meshes.

	Figure 13 Mesh A				Figure 2 Mesh			
h	$\|\mathbf{e_u}\|_{1,\Omega}$	$\|e_p\|_{0,\Omega}$	$\|\mathbf{e_u}\|_{l_\infty}$	$\|e_p\|_{l_\infty}$	$\|\mathbf{e_u}\|_{1,\Omega}$	$\|e_p\|_{0,\Omega}$	$\|\mathbf{e_u}\|_{l_\infty}$	$\|e_p\|_{l_\infty}$
$\frac{1}{4}$	0.1486	0.1119	0.00884	0.2050	0.1484	0.1124	0.0282	0.3586
$\frac{1}{8}$	0.0403	0.0249	0.00201	0.0571	0.0406	0.0366	0.0063	0.1523
$\frac{1}{16}$	0.0102	0.0049	0.00053	0.0194	0.0102	0.0136	0.0017	0.0813
α ($O(h^\alpha)$)	1.9	2.2	2.0	1.7	1.9	1.5	2.0	1.0

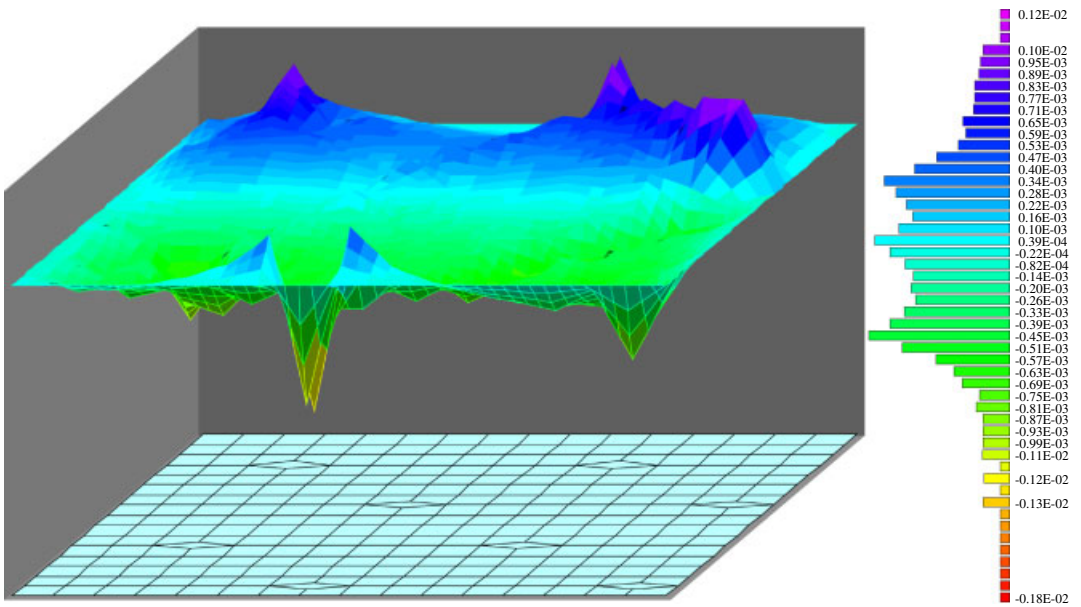

Figure 15. Component 1 of $\mathbf{e_u}$ on a selectively stabilized mesh.

However, the maximal nodal error $|\mathbf{u} - \mathbf{u}_h|_{l^\infty}$ for the former is 0.0024, much bigger than that of latter, 0.00178.

Our third test is to check our second idea, perturbing one vertex of each patch of squares, shown in Figure 3. The error is plotted in Figure 16. Again, we perturb one internal vertex of a $\mathscr{M}_{2h}$ square out of every eight $\mathscr{M}_{2h}$ squares. We note that, compared to the second numerical test above, the number of nodal variables for the velocity is reduced further from 466 to 450. However, the maximal nodal error $|\mathbf{u} - \mathbf{u}_h|_{l^\infty}$ is even smaller, from 0.00178 to 0.00088.

The next numerical test is to check the uniform grids, as depicted in Figure 13 Mesh A. In this case, the resulting linear system is singular and we have to filter out the checkerboard mode pressure. The error of the component one of the velocity is plotted in Figure 17. The error is smooth, and smaller than that of three earlier tests. The maximal nodal error $|\mathbf{u} - \mathbf{u}_h|_{l^\infty}$ is 0.00053

DOI: 10.1002/fld

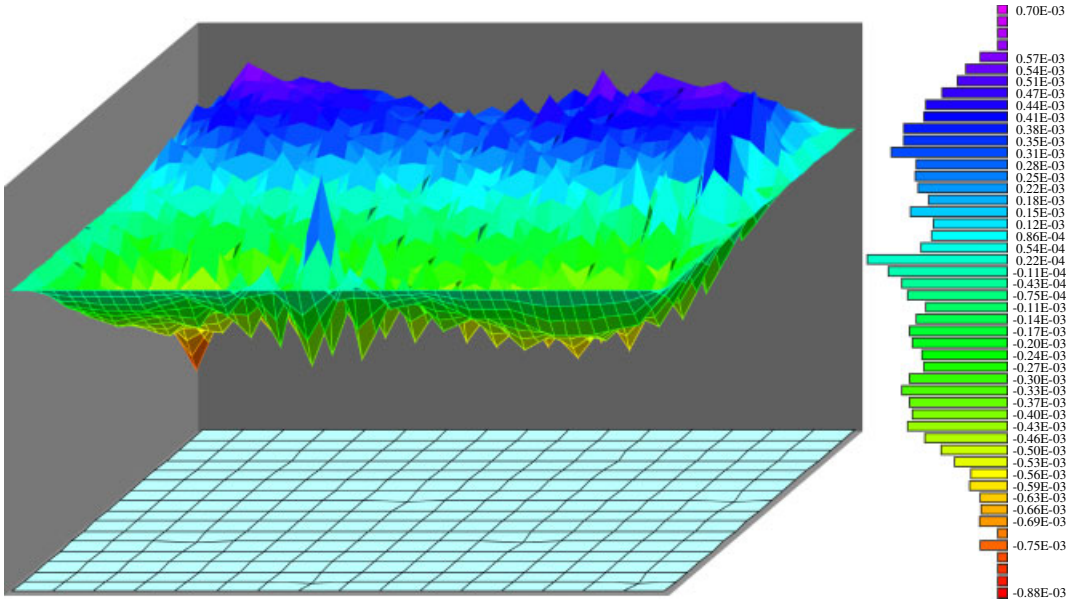

Figure 16. Component 1 of $\mathbf{e_u}$ on a selectively perturbed mesh.

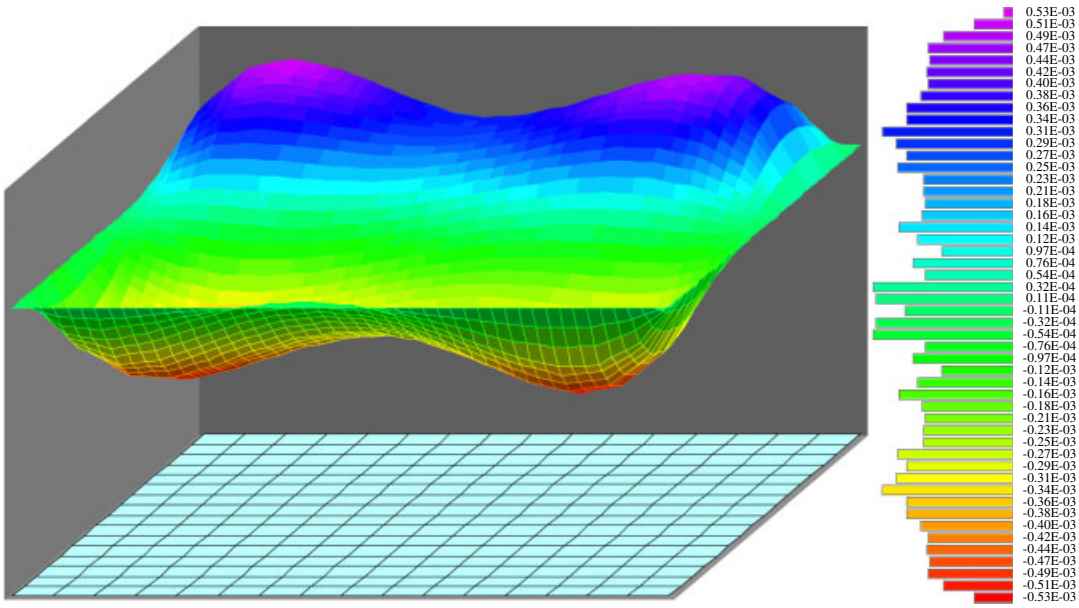

Figure 17. Component 1 of $\mathbf{e_u}$ on the uniform mesh.

DOI: 10.1002/fld

Table III. Inf–sup constants and accuracy of $\mathscr{Q}_1$–$\mathscr{P}_0$ and the stabilizations.

	Figure 13 Mesh A			Figure 5 Mesh			Figure 4 Mesh		
h	$\|\mathbf{e_u}\|_\infty$	$\|e_p\|_\infty$	$\bar{\gamma}_h$	$\|\mathbf{e_u}\|_\infty$	$\|e_p\|_\infty$	γ_h	$\|\mathbf{e_u}\|_\infty$	$\|e_p\|_\infty$	γ_h
$\frac{1}{4}$	0.00884	0.08026	0.13513	0.00884	0.21139	0.02408	0.00884	0.09411	0.01438
$\frac{1}{8}$	0.00201	0.03253	0.04661	0.00754	0.22433	0.04086	0.00295	0.09705	0.01777
$\frac{1}{16}$	0.00053	0.01060	0.01318	0.00145	0.16360	0.04477	0.00077	0.07171	0.01899
$\frac{1}{32}$	0.00013	0.00298	0.00346	0.00025	0.10034	0.04507	0.00017	0.04981	0.02322

in this case. We list the convergence results for the uniform meshes in the left part of Table II. At the end, we test the methods shown in Figures 4 and 5. For both cases, we obtain graphs almost identical to Figure 17, and obtain errors very close to those listed in Table II for the uniform meshes. We omit the details here. Further study and discussion on these two methods, and their generalizations, would appear somewhere else. We compare the inf–sup constants and the accuracy of the two methods to those of the standard element, by Table III.

ACKNOWLEDGEMENT

The first author would like to thank Prof. Douglas N. Arnold for his encouragement, advice, and support during the years of the author's study at the Pennsylvania State University.

REFERENCES

1. Brezzi F, Fortin M. *Mixed and Hybrid Finite Element Methods*. Springer: Berlin, 1991.
2. Raviart PA, Girault V. *Finite Element Methods for Navier–Stokes Equations*. Springer: Berlin, 1986.
3. Babuška I. The finite element method with Lagrangian multipliers. *Numerical Mathematics* 1973; **20**:179–192.
4. Brezzi F. On the existence, uniqueness, and approximation of saddle point problems arising from Lagrangian multipliers. *RAIRO* 1974; **8**:129–151.
5. Boland JM, Nicolaides RA. Stability of finite elements under divergence constraints. *SIAM Journal on Numerical Analysis* 1983; **20**:722–731.
6. Boland JM, Nicolaides RA. Stable and semistable low order finite elements for viscous flows. *SIAM Journal on Numerical Analysis* 1985; **22**:474–492.
7. Griffiths D, Silvester D. Unstable modes of the Q_1–P_0 element. *Numerical Analysis Report No. 257*, Department of Mathematics, University of Manchester, 1994.
8. Johnson C, Pitkäranta J. Analysis of some mixed finite element methods related to reduced integration. *Mathematics of Computation* 1982; **158**:375–400.
9. Malkus DS. Eigenproblems associated with the discrete LBB-condition for incompressible finite elements. *International Journal for Engineering Science* 1981; **19**:1299–1310.
10. Mansfield L. On finite element subspaces on quadrilateral and hexahedral meshes for incompressible viscous flow problems. *Numerical Mathematics* 1984; **45**:165–172.
11. Pitkäranta J, Stenberg R. Analysis of some mixed finite element methods for plane elasticity equations. *Mathematics of Computation* 1983; **41**:399–423.
12. Oden JT, Jacquotte O. Stability of some mixed finite element methods for Stokesian flows. *Computational Methods in Applied Mechanics and Engineering* 1984; **43**:231–247.
13. Pitkäranta J, Stenberg R. Error bounds for the approximation of the Stokes problem using bilinear/constant elements on irregular quadrilateral meshes. In *The Mathematics of Finite Elements and Applications V*, Whiteman J (ed.). Academic Press: London, 1985; 325–334.

DOI: 10.1002/fld

14. Sani RL, Gresho PM, Lee RL, Griffiths D. The cause and cure(!) of the spurious pressures generated by certain FEM solutions of the incompressible Navier–Stokes equations. *International Journal for Numerical Methods in Fluids* 1981; **1**:171–204.
15. Stenberg R. Analysis of mixed finite element methods for the Stokes problem: a unified approach. *Mathematics of Computation* 1984; **42**:9–23.
16. Eguchi Y. A new positive-definite regularization of incompressible Navier–Stokes equations discretized with Q1/P0 finite element. *International Journal for Numerical Methods in Fluids* 2003; **41**:881–904.
17. Silvester DJ, Kechkar N. Stabilised bilinear-constant velocity–pressure finite elements for the conjugate gradient solution of the Stokes problem. *Computer Methods in Applied Mechanics and Engineering* 1990; **79**:71–86.
18. Hughes T, Franca LP. A new finite element formulation for computational fluid dynamics: VII the Stokes problem with various well-posed boundary conditions: symmetric formulations that converge for all velocity/pressure spaces. *Computer Methods in Applied Mechanics and Engineering* 1987; **65**:85–96.
19. Stenberg R. Error analysis of some finite element methods for the Stokes problem. *Mathematics of Computation* 1990; **54**:495–508.
20. Arnold DN, Qin J. Quadratic velocity/linear pressure Stokes elements. In *Advances in Computer Methods for Partial Differential Equations VII*, Vichnevetsky R, Steplemen RS (eds). 1992.
21. Qin J. On the convergence of some low order mixed finite elements for incompressible fluids. *Thesis*, Pennsylvania State University, 1994.
22. Clement P. Approximation by finite element functions using local regularization. *RAIRO Analyse Numerique* 1975; **R-2**:77–84.
23. Scott LR, Zhang S. Finite element interpolation of nonsmooth functions satisfying boundary conditions. *Mathematics of Computation* 1990; **54**:483–493.
24. Le Tallec P, Ruas V. On the convergence of the bilinear-velocity constant-pressure finite element method in viscous flow. *Computer Methods in Applied Mechanics and Engineering* 1986; **54**:235–243.

DOI: 10.1002/fld